Article:
Helmig, Detlev, Rossabi, Samuel, Hueber, Jacques et al. (18 more authors) (2016) Reversal of global atmospheric ethane and propane trends largely due to US oil and natural gas production. Nature Geoscience. 490–495. ISSN 1752-0908

https://doi.org/10.1038/ngeo2721

Revised version – April 22, 2016

Manuscript in press as 'Letter to Nature'

Reversal of Global Atmospheric Ethane and Propane Trends largely due to US Oil and Natural Gas Production

Detlev Helmig[1], Samuel Rossabi[1], Jacques Hueber[1], Pieter Tans[2], Stephen A. Montzka[2], Ken Masarie[2], Kirk Thoning[2], Christian-Plass Duelmer[3], Anja Claude[3], Lucy J. Carpenter[4], Alastair C. Lewis[5], Shalini Punjabi[4], Stefan Reimann[6], Martin K. Vollmer[6], Rainer Steinbrecher[7], James W. Hannigan[8], Louisa K. Emmons[8], Emmanuel Mahieu[9], Bruno Franco[9], Dan Smale[10], Andrea Pozzer[11]

Non-methane hydrocarbons such as ethane are important precursors to tropospheric ozone and aerosols. Using data from a global surface network and atmospheric column observations we show that the steady decline in ethane concentrations that began in the 1970s[1-3] halted between 2005 and 2010 in most of the Northern Hemisphere, and has since reversed. We calculate a yearly increase in ethane emissions in the Northern Hemisphere of 0.42 (± 0.19) Tg yr^{-1} between mid-2009 and mid-2014. The largest increases in ethane and for the shorter-lived propane are seen over the central and eastern USA, with a spatial distribution that suggests North American oil and natural gas development as the primary source of increasing emissions. By including other co-emitted oil and natural gas non-methane hydrocarbons, we estimate a Northern Hemisphere total non-methane hydrocarbons yearly emission increase of 1.2 (± 0.8) Tg yr^{-1}. Atmospheric chemical transport modeling suggests these emissions could augment summertime mean surface ozone by several nmol mol^{-1} near oil and natural gas production regions. Methane/ethane oil and natural gas emission ratios suggest a significant increase in associated methane emissions; however, this increase is inconsistent with observed leak rates in production regions and changes in methane's global isotopic ratio.

[1]Institute of Arctic and Alpine Research, University of Colorado, Boulder, USA; [2]Earth Systems Research Laboratory, National Oceanic and Atmospheric Administration, Boulder, USA; [3]Deutscher Wetterdienst, Hohenpeissenberg, Germany; [4]Wolfson Atmospheric Chemistry Laboratories, University of York, United Kingdom, [5]National Centre for Atmospheric Science, University of York, United Kingdom; [6]Laboratory for Air Pollution and Environmental Technology, Empa, Swiss Federal Laboratories for Materials Science and Technology, Duebendorf, Switzerland; [7]Karlsruhe Institute for Technology, Campus Alpine, Garmisch-Partenkirchen, Germany; [8]National Center for Atmospheric Research, Boulder, USA; [9]Institute of Astrophysics and Geophysics, University of Liège, Belgium; [10]National Institute of Water and Atmospheric Research, Lauder, New Zealand; [11]Max Planck Institute for Chemistry, Mainz, Germany.

Oxidation of atmospheric non-methane hydrocarbons (NMHCs) contributes to production of surface ozone and secondary aerosol, both of which impact air quality and climate. NMHCs are emitted into the atmosphere from a variety of biogenic and anthropogenic sources. Ethane is the longest-lived and most abundant NMHC found typically at ~0.4–2.5 nmol mol^{-1} (ppb) in the background atmosphere. It is released from seepage of fossil carbon deposits, volcanoes, fires, and from human activities, with fossil fuel extraction, distribution leakage, and industrial use being the major sources. Pre-industrial ethane atmospheric mole fractions measured in polar ice cores were between ~1/4 -1/2 of current levels, i.e. ~400 pmol mol^{-1} in the northern hemisphere (NH), and ~100 pmol mol^{-1} in the southern hemisphere (SH)[4]. In the early part of the 20th century NMHCs increased steadily in the global atmosphere. Firn air records[1-3] show that light alkane NMHC (C_2-C_5) increased post-1950 and reached a maximum that was ~50% above 1950 levels during 1970–1985. Global atmospheric ethane peaked around 1970. NMHC have since been steadily declining to concentrations that are close to the earliest data in the record ([1] and Fig. 1(a)). These trends are primarily due to stricter air quality emission controls that were first implemented some 50 years ago with the goal to reduce human exposure to NMHCs and surface ozone. The regulations resulted in reduced emissions from sources, such as the O&NG industries and automobiles, and a gradual decline of atmospheric NMHCs in urban air in many developed countries and also in the background atmosphere[5-7].

Ethane and methane are co-emitted from oil and natural gas (O&NG) sources. Ethane observations have been used to attribute anthropogenic methane emission changes[7]. Having the longest NMHC lifetime, on the order of 2 (summer) to 6 (winter) months, ethane is the NMHC observed with the least spatial and short-term variability in background air, making it the best candidate species for studying hemispheric gradients and long-term changes.

We analyzed ten years of NMHC data collected at 44 remote global sampling sites from NOAA's Global Greenhouse Gas Reference Network (GGGRN). We also include data from *in-situ* monitoring at Summit, Greenland[8], at Hohenpeissenberg (HPB) in Southern Germany[9], Jungfraujoch

(JFJ) and Rigi (RIG), Switzerland, and Cape Verde in the mid-Atlantic[10]. For propane, we further included results from eight sites within NOAA's GGGRN (Methods).

Atmospheric NMHC display a dynamic seasonal and latitudinal behavior. Maxima are seen in late winter, and minima in the summer (Fig. 1). Sources of light NMHC do not vary much seasonally[11]; seasonal cycles are primarily driven by photochemical loss. Consequently, seasonal cycles exhibit the largest amplitude near the poles, are small near the equator (Fig. 2), and are shifted by ~6 months in the SH due to the opposite season. There is also a strong latitudinal gradient of absolute values, with highest abundances observed in the Arctic, steeply declining levels at mid-latitudes, and lower abundance in the SH. These gradients are caused by sources that are dominated by anthropogenic emissions, which are highest in the industrialized mid-northern latitudes, and the slower transport across the equatorial zone compared to within-hemisphere mixing. Gases with shorter lifetimes, i.e. propane, *i*-butane, *n*-butane, display more pronounced seasonal and latitudinal gradients (Fig. 2).

Individual site data reveal that for many NH locations the downward trends reported in earlier work has halted and reversed to increasing NMHC levels. Because the flask network program started in 2006, data for most sites do not go back far enough for deciphering the exact time of the trend reversal. The second order polynomial fit through the longest, and most highly time resolved *in-situ* record from HPB has its minimum in 2009 (Fig. 1 (e)), in agreement with the JFJ FTIR column observations (Fig. 1(c)). Focusing on the most recent five years (2009.5 – 2014.5) we find variable results in the observed rate of change; however, a consistent picture emerges that shows the largest increases at NH sites (Fig. 3). Of 33 NH sites, 7 exhibit ethane growth rates > 50 pmol $mol^{-1}yr^{-1}$, and 10 sites exhibit growth rates between 25-50 $pmol^{-1}yr^{-1}$ (Table S1). Depending on grouping of sites and averaging across regions and calculation method a mean NH ethane increase rate of 2.9 - 4.7% yr^{-1} is calculated (Methods). These rates of change in atmospheric ethane have not been seen at SH sites; most SH sites show only small changes, with poorer regression results. Applying a 2^{nd} order polynomial fit to the NH trend curve results yields positive quadratic coefficients in 22 out of 31 cases, showing that for the majority of cas-

es, ethane trend curves are becoming steeper, i.e. rates of change in atmospheric abundance have been increasing at most of the sites during this time window.

This hemispheric difference in ethane trends is further supported by two contrasting records of ethane column observations (i.e. the average from the ground to the top of the atmosphere), one from JFJ (Fig. 1(c))[12], and the other one from Lauder, New Zealand (Fig. 1(d)). At the 3,580 m elevation of JFJ, these data are a good representation of free tropospheric ethane, reflecting the continental background and long range transport. While there was a slight downward trend in the data for the first 15 years of the record, in agreement with the trends inferred from the firn and HPB data, a reversal is evident after 2009, with a post-2009 rate of increase in the mid-troposphere of 4.2 ± 1.0 % yr^{-1}. The upward trend is evident in both the mid-troposphere and upper troposphere/lower stratosphere partial columns, indicative of the hemispheric nature of the ethane increase. The ethane trend reversal is absent in the SH FTIR column data (Fig. 1(d)). The difference in trends in the hemispheres is consistent with an increasing NH source.

Notably, ethane rates of change are highest at the central and eastern USA and nearby downwind sites, suggesting the ethane increase is driven to a large part by emissions from North America. The regional hotspot of increasing NMHC levels can be pinpointed more narrowly from propane observations. Propane, with a lifetime ~1/4 of ethane, is a more sensitive indicator for local/regional emissions. Propane data show the greatest increases in the central and eastern USA and in the downwind North Atlantic Region (Fig. 3). In contrast, propane levels have been relatively stable in central Europe, the Pacific region, and the SH. Also, measurements in the western USA do not show propane increases. With the primary synoptic transport direction being west and south-west to east, the spatial analyses of ethane and propane increases point to the central to eastern parts of the USA as the regions where most of the emission increases have occurred.

The O&NG sector is a major source of light NMHC emissions. A surge in O&NG production has occurred in recent years, particularly in the USA, where unconventional oil and natural gas drilling has resulted in estimated 10-20-fold increases in shale O&NG production between 2000 and 2015 (www.eia.gov), making the USA the fastest growing and a leading O&NG producing na-

tion. Ground and airborne observations have consistently shown elevated levels of methane and NMHC as a result of venting, flaring, and leakage. NMHC ambient concentrations measured in oil and gas basins can far exceed (up to > 100 times) the regional background or indeed urban and other industrial regions. Top-down emission estimates are well above inventory estimates[13-17]. Resulting ozone production from these emissions has led to air quality standard exceedances in the Uintah Basin, UT, and Upper Green River Basin, WY, O&NG regions[18,19]. Two other regional studies have previously noted upwards trends in ambient NMHC and associated these changes to upwind O&NG activities. Vinciguerra et al.[20] reported an increase from 7% to 13% of the total observed non-methane organic carbon abundance during 2010 to 2013, and increasing ethane mixing ratios based on measurements in Baltimore, MD, downwind of the Marcellus Shale. Similarly, Schade et al.[21], analyzing data from southern Texas, reported steeply increasing ethane levels associated with transport from the Eagle Ford Shale.

Applying the JFJ FTIR mid-troposphere column trend value of 4.2% yr^{-1} to the NH annual ethane emission estimate of 9.9 Tg yr^{-1} (Methods) yields an estimate for an ethane annual emission increase of 0.42 ± 0.19 Tg yr^{-1} (per year; see Methods for all uncertainty range calculations), resulting in an overall 2.1 ± 1.0 Tg yr^{-1} emission increase since 2009.5. This additional emission is ~1.5 times the NA inventory estimate of 1.6 Tg yr^{-1} for 2007. Considering estimates of co-emitted NMHC yields an estimate for a total NMHC emissions increase of 1.2 ± 0.8 Tg yr^{-1} (per year; 5.9 ± 4.0 Tg yr^{-1} overall emissions increase during 2009.5 – 2014.5).

There is no evidence for major non-O&NG NMHC emissions increases. From the spatial overlap of USA O&NG regions with identified areas of largest NMHC increases it appears likely that the NMHC increase is largely driven by USA O&NG production. This added NMHC emission is expected to fuel additional surface ozone production in source and downwind regions. Figure 4 illustrates modeling results from a first-order of magnitude sensitivity study, where the 4.2% yr^{-1} increase in the C_2-C_5 NMHC flux was attributed to USA O&NG emissions over five years at constant emissions of nitrogen oxides (NO_x). This added emission causes changes in surface ozone in regions with O&NG development and downwind, reaching up to 0.5 nmol mol^{-1} yr^{-1} (per year) average ozone increases for June – August, corresponding to 2.5 nmol mol^{-1} increases

overall over the five year period simulated with the model. The sensitivity is particularly high in the western USA, mostly driven by higher NO_x in that region. Consequently, these NMHC emission changes can potentially offset emission controls that have been implemented for curbing photochemical ozone production, and therefore can be a concern for attaining the ozone air quality standard.

Atmospheric methane has been increasing since ~2007, after a ~8 year period of stable levels. Continental emission changes in methane are difficult to decipher because of the variety of biological, burning, and O&NG related emissions, and the fact that trends are small relative changes in the large methane background. With shorter atmospheric lifetimes, trends of NMHC are more noticeable on a regional scale. Methane and ethane are co-emitted from O&NG sources in mass ratios of 1.7–33, with most results ranging from 7-14 (Table S5). If we assume that the added ethane emission is entirely from O&NG sources, that the methane/ethane ratio from O&NG has not changed over time, and considering a median source region methane/ethane emission ratio of 10, an increase in the anthropogenic methane emission of 4.4 ± 3.1 Tg yr^{-1} is estimated for the NH each year during 2009.5–2014.5. The cumulative increase in methane emissions implied from this approach would represent more than a doubling of O&NG related methane USA inventory emissions[22] and a ~6.2% total increase between 2009.5–2014.5 of the 330 Tg yr^{-1} [23] global anthropogenic methane emission. While other recent studies[12,24,25,26] have derived similar estimates for methane emission increases and associated those to increased NA O&NG emissions, most also rely on the extrapolation of NMHC results to infer methane emission changes. We note that surface and aircraft observations of methane stable isotopes from the GGGRN are inconsistent with such a large NA methane flux increase from O&NG sources[27]. Furthermore, the methane emission implied by this analysis of NMHC data as a fraction of O&NG production is a substantially higher percentage than what has been observed in O&NG fields in North America[13,17,28-30]. This suggests yet unidentified increasing sources for NMHC emissions independent of methane or with lower methane/ethane emission ratios, or potential emission increases outside of NA that currently cannot be well defined due to the sparsity of observations in those regions (for instance in the middle-East, Africa, and Asia).

172 _____

173 **Author Contributions Statement:**

174 DH: Study design, global flask network operation, Summit in-situ measurements, data analyses,
175 quality control, site comparisons, manuscript preparation
176 SR: Data processing, preparation of graphs, manuscript preparation
177 JH: Global flask network operation, analytical work, Summit in-situ measurements
178 PT: Global flask network operation, manuscript preparation
179 SAM: North American Tower flask program management and data processing/quality control,
180 manuscript preparation
181 KM: NOAA network data management, NMHC global graphs shown in Fig. 2, manuscript prepa-
182 ration
183 KT: Data filtering, trend analyses, data statistics, manuscript preparation
184 CPD: HPB NMHC monitoring, flask-in-situ comparisons, manuscript preparation
185 AC: HPB in-situ NMHC monitoring
186 ACL: CVO NMHC in-situ observations, manuscript preparation
187 LC: CVO NMHC in-situ observations, manuscript preparation
188 SP: CVO NMHC in-situ observations
189 SR: JFJ NMHC in-situ observations
190 MKV, JFJ NMHC in-situ observations, manuscript preparation
191 RS: VOC World Calibration Center, NMHC quality control, manuscript preparation
192 JE, FTIR data evaluations and coordination, manuscript preparation
193 LKE, Emissions modeling, ethane inventory data, manuscript preparation
194 JWH: FTIR observations and data processing, manuscript preparation
195 EM: JFJ FTIR data processing and analyses, manuscript preparation
196 BF: JFJ FTIR data processing and analyses, manuscript preparation
197 DS: Lauder FTIR observations and data processing, manuscript preparation
198 AP: Ethane inventory data, photochemical ozone modeling, manuscript preparation
199

Requests for materials should be addressed to Detlev Helmig, detlev.helmig@colorado.edu

Data Sources:

http://www.esrl.noaa.gov/gmd/dv/data/

http://ds.data.jma.go.jp/gmd/wdcgg/

ftp://ftp.cpc.ncep.noaa.gov/ndacc/station/

Acknowledgements:

This research would not have been possible without the contributions of many dedicated researchers that maintain the sampling programs that provided the used data. The global VOC flask analyses are a component of NOAA's Cooperative USA - and global-scale Greenhouse Gas Reference flask sampling network, which is supported in part by NOAA Climate Program Office's AC4 Program. We greatly appreciate the work of many colleagues who have contributed to the program operation and data processing, in particular C. Siso, P. Lang, J. Higgs, M. Crotwell, S. Wolter, D. Neff, J. Kofler, A. Andrews, B. Miller, D. Colegrove, C. Sweeney, E. Dlugokencky, and Y. Stenzel, and many unnamed CU Boulder undergraduate students who have processed the flask sampling network data. We thank M. Fischer and S. Biraud for the operation of the STR and SGP site, respectively. The WGC and STR sites are operated with support from the California Energy Commission's Natural Gas program under USA Department of Energy Contract No. DE-AC02-05CH11231. The monitoring at Summit is funded by the National Science Foundation grant OPP AON 1108391. Financial support for the measurements at JFJ is provided by the International Foundation High Altitude Research Stations JFJ and Gornergrat (HFSJG), and for the GC/MS measurements also by the Swiss Federal Office for the Environment (FOEN) in the Swiss National Program HALCLIM. In-situ VOC measurements at Cape Verde are made with the assistance of L. Mendes, K. Read, and J. Hopkins. The University of York thanks NCAS and NERC for funding. The FTIR measurements at NIWA, Lauder are core funded through New Zealand's Ministry of Business, Innovation and Employment. J. Hannigan is supported by NASA under contract. The National Center for Atmospheric Research is supported by the National Science Foundation. The University of Liège contribution has been primarily supported by BELSPO and the F.R.S. – FNRS (Fonds de la Recherche Scientifique), both in Brussels. The reconstructed ethane firn air history shown in Fig. 1(a) were calculated by P. Martinerie, at LGGE, Grenoble, and were previously published in [1]. The global VOC monitoring is under the auspices of the World

Meteorological Organization Global Atmospheric Watch (WMO-GAW) program, which facilitates coordination between participating partners and quality control efforts. The WCC-VOC is funded by the German Umweltbundesamt. We also thank the staff of the World Data Centre for Greenhouse Gases at the Japan Meteorological Agency for the archiving and public posting of data used in this study.

Corresponding Author: Detlev Helmig, Institute of Arctic and Alpine Research, University of Colorado, Boulder, USA; 001 303 492-2509, detlev.helmig@colorado.edu

References for Main Text

1 Aydin, M. *et al.* Recent decreases in fossil-fuel emissions of ethane and methane derived from firn air. *Nature* **476**, 198-201, doi:10.1038/nature10352 (2011).

2 Worton, D. R. *et al.* Evidence from firn air for recent decreases in non-methane hydrocarbons and a 20th century increase in nitrogen oxides in the northern hemisphere. *Atmos. Environ.* **54**, 592-602 (2012).

3 Helmig, D. *et al.* Reconstruction of Northern Hemisphere 1950-2010 atmospheric non-methane hydrocarbons. *Atmos. Chem. Phys.* **14**, 1463-1483, doi:10.5194/acp-14-1463-2014 (2014).

4 Nicewonger, M.R, Verhulst, K.R, Aydin, M., & Saltzman, E. S. Preindustrial atmospheric ethane levels inferred from polar ice cores: A constraint on the geologic sources of atmospheric ethane and methane. *Gephys. Res. Lett.* **43**, 10.1002/2015GL066854 (2015).

5 Von Schneidemesser, E., Monks, P. S. & Plass-Duelmer, C. Global comparison of VOC and CO observations in urban areas. *Atmos. Environ.* **44**, 5053-5064, doi:10.1016/j.atmosenv.2010.09.010 (2010).

6 Warneke, C. *et al.* Multiyear trends in volatile organic compounds in Los Angeles, California: Five decades of decreasing emissions. *J. Geophys. Res.* **117**, doi:D00v1710.1029/2012jd017899 (2012).

7 Simpson, I. J. *et al.* Long-term decline of global atmospheric ethane concentrations and implications for methane. *Nature* **488**, 490-494, doi:10.1038/nature11342 (2012).

8 Kramer, L. J. *et al.* Seasonal variability of atmospheric nitrogen oxides and non-methane hydrocarbons at the GEOSummit station, Greenland. *Atmos. Chem. Phys.* ***12***, 6827-6849.

9 Plass-Duelmer, C., Michl, K., Ruf, R. & Berresheim, H. C-2-C-8 hydrocarbon measurement and quality control procedures at the Global Atmosphere Watch Observatory Hohenpeissenberg. *J. Chrom.* **953**, 175-197, doi:10.1016/s0021-9673(02)00128-0 (2002).

10 Read, K. A. *et al.* Intra-annual cycles of NMVOC in the tropical marine boundary layer and their use for interpreting seasonal variability in CO. *J. Geophys. Res.* **114**, doi:10.1029/2009jd011879 (2009).

11 Leuchner, M. *et al.* Can positive matrix factorization help to understand patterns of organic trace gases at the continental Global Atmosphere Watch site Hohenpeissenberg? *Atmos. Chem. Phys.* **15**, 1221-1236, doi:doi:10.5194/acp-15-1221-2015 (2015).

12 Franco, B. *et al.* Retrieval of ethane from ground-based FTIR solar spectra using improved spectroscopy: Recent burden increase above Jungfraujoch. *J. Quant. Spec. & Rad. Trans.* **160**, 36-49, doi:10.1016/j.jqsrt.2015.03.017 (2015).

13 Pétron, G. *et al.* Hydrocarbon emissions characterization in the Colorado Front Range: A pilot study. *J. Geophys. Res.-Atmospheres* **117**, 1-19, doi:10.1029/2011jd016360 (2012).

14 Helmig, D. *et al.* Highly Elevated Atmospheric Levels of Volatile Organic Compounds in the Uintah Basin, Utah. *Environ. Sci. Technol.* **48**, 4707-4715, doi:10.1021/es405046r (2014).

15 Thompson, C. R., Hueber, J. & Helmig, D. Influence of oil and gas emissions on ambient atmospheric non-methane hydrocarbons in residential areas of Northeaster Colorado. *Elementa* **2**, 1-16, doi:10.12952/journal.elementa.000035 (2014).

16 Swarthout, R. F. *et al.* Impact of Marcellus Shale Natural Gas Development in Southwest Pennsylvania on Volatile Organic Compound Emissions and Regional Air Quality. *Environ. Sci. Technol.* **49**, 3175-3184, doi:10.1021/es504315f (2015).

17 Karion, A. *et al.* Methane emissions estimate from airborne measurements over a western United States natural gas field. *Geophys. Res. Lett.* **40**, 1-5, doi:10.1002/grl.50811 (2013).

18 Schnell, R. C. *et al.* Rapid photochemical production of ozone at high concentrations in a rural site during winter. *Nature Geoscience* **2**, 120-122, doi:10.1038/ngeo415 (2009).
19 Oltmans, S. *et al.* Anatomy of wintertime ozone associated with oil and natural gas extraction activity in Wyoming and Utah. *Elementa* **2**, doi: 10.12952/journal.elementa.000024 (2014).
20 Vinciguerra, T. *et al.* Regional air quality impacts of hydraulic fracturing and shale natural gas activity: Evidence from ambient VOC observations. *Atmos. Environ.* **110**, 144-150, doi:10.1016/j.atmosenv.2015.03.056 (2015).
21 Schade, G. W. & Roest, G. S. Is the shale boom reversing progress in curbing ozone pollution? *EOS* **96**, doi:10.1029/2015EO028279 (2015).
22 EPA. US Greenhouse Gas Inventory. *https://www3.epa.gov/climatechange/ghgemissions/index.html* (accessed March 2016).
23 Kirschke, S. *et al.* Three decades of global methane sources and sinks. *Nature Geoscience* **6**, 813-823, doi:10.1038/ngeo1955 (2013).
24 Franco, B. *et al.* Evaluating ethane and methane emissions associated with the development of oil and natural gas extraction in North America. *Environ. Res. Lett.* **11**, 044010 (2016).
25 Hausmann, P., Sussmann, R. & Smale, D. Contribution of oil and natural gas production to renewed increase of atmospheric methane (2007–2014): top-down estimate from ethane and methane column observations. *Atmos. Chem. Phys.* **16**, 3227-3244 (2016).
26 Turner, A. J. *et al.* A large increase in US methane emissions over the past decade inferred from satellite data and surface observations. *Geophys. Res. Lett.* **43**, 2218–2224, doi:10.1002/2016GL067987 (2016).
27 Schaefer, H. *et al.* A 21st century shift from fossil-fuel to biogenic methane emissions indicated by 13CH4. *Science* 10.1126/science.aad2705 (2016).
28 Peischl, J. *et al.* Quantifying atmospheric methane emissions from the Haynesville, Fayetteville, and northeastern Marcellus shale gas production regions. *J. Geophys. Res.* **120**, 2119-2139, doi:10.1002/2014jd022697 (2015).
29 Karion, A. *et al.* Aircraft-Based Estimate of Total Methane Emissions from the Barnett Shale Region. *Environ. Sci. & Technol.* **49**, 8124-8131, doi:10.1021/acs.est.5b00217 (2015).
30 Petron, G. *et al.* A new look at methane and nonmethane hydrocarbon emissions from oil and natural gas operations in the Colorado Denver-Julesburg Basin. *J. Geophys. Res.* **119**, 6836-6852, doi:10.1002/2013jd021272 (2014).

Methods

Global VOC Network. Since 2004 the NOAA GMD and INSTAAR in Boulder, CO, have been operating a global volatile organic compound (VOC) monitoring program that is building on the NOAA Global Greenhouse Gas Reference Network (GGGRN). VOC are quantified in whole air sampled in pairs of glass flasks that are collected weekly to bi-weekly at ~44 global background monitoring sites, with a total sample number of ~3000 per year. Ethane, acetylene, propane, *iso*-butane, *n*-butane, *iso*-pentane, *n*-pentane, isoprene, benzene, and toluene are currently analyzed in the sample remaining in the flasks after completion of analyses of greenhouse gases, and of CO_2 and methane stable isotopic ratios. The gas chromatography (GC) with flame ionization detection method [1] is calibrated by a series of gravimetrically prepared synthetic and whole air standards. The program operates under the umbrella of the WMO-GAW and is collaborating with international partners on exchange of calibration standards and comparison of calibration scales[2]. The INSTAAR lab was audited by the World Calibration Center (WCC) for VOC[3] in 2008 and 2011. Five unknown standards were analyzed and results reported to the WCC. Mean results of five repeated measurements of the provided standards deviated <1.5% ethane, and < 0.8% for propane from the certified values. These deviations are well below the deviation criteria set by GAW[4]. Uncertainties in the NMHC data are estimated to be ≤ 5% for results > 100 pmol mol^{-1} and ≤ 5 pmol mol^{-1} for results < 100 pmol mol^{-1}. More analytical and program details are provided by [1,5,6].

VOC *in-situ* monitoring at Summit (SUM), Greenland. Year-round VOC monitoring at Summit (72.6° N, 38.5° W; 3216 m asl) was performed from 26 June 2008 to 22 July 2010, totaling 756 days (just over 2 years) [7], and has been resumed in May 2012. The GC is calibrated several times per week using standards that are cross-referenced against the global flask network laboratory scale. Uncertainties in the NMHC data are estimated to be ≤ 5% for results > 100 pmol mol^{-1} and ≤ 5 pmol mol^{-1} for results < 100 pmol mol^{-1}.

VOC *in-situ* monitoring at Hohenpeissenberg (HPB). Continuous VOC monitoring at HPB (47.8°N, 11.8°E, 980 m asl) has been conducted since 1998 as part of the WMO-GAW[8]. Calibrations rely on a series of gravimetric and whole air standards referenced to the WCC. VOC sam-

pling is conducted daily at noontime. Uncertainties (95% confidence interval) are generally ± (1.9 pmol mol^{-1} + 2.9%) in the ethane mole fraction, and ± (1.3 pmol mol^{-1} + 2.9%) for propane, except for isolated periods of degraded chromatography or other instrumental issues which results in higher uncertainties. Detection limits are at ~3 and 2 pmol mol^{-1} for ethane and propane, respectively.

VOC *in-situ* monitoring at Jungfraujoch (JFJ). At JFJ, a high elevation site in the central Swiss Alpes (46.5°N, 7.6°E, 3466 m asl), VOC are measured using a Medusa GC/mass spectrometer (MS)[9] hourly with each pair of measurements bracketed by standard measurements. Ethane and propane measurements started in 2008 and are ongoing. Measurement precisions are 0.3% for ethane and 0.8 % for propane (1 σ). Calibration is provided by referencing standards against primary reference gases of the National Physical Laboratories (UK) and thus is linked to the WMO-VOC scale. Uncertainties are ~10 % for ethane and 3% for propane.

VOC *in-situ* monitoring at Cape Verde (CVAO). The Cape Verde Atmospheric Observatory (CVAO) Humberto Duarte Fonseca (16.8°N, 24.9°W, 10 m asl) is positioned upwind of Calhau on the northeastern side of São Vicente, Cape Verdes. Hourly VOC measurements are made from a height of 20 m asl; analytical details are provided by [10]. Uncertainties in the NMHC data are estimated to be ≤ 5% for results > 100 pmol mol^{-1}, and ≤ 5 pmol mol^{-1} for results <100 pmol mol^{-1}. Detection limits are 2.6 and 1.6 pmol mol^{-1} for ethane and propane, respectively. Calibrations are linked to the WMO-VOC scale.

VOC measurements from North American tower sites. Glass flasks are also collected with automated samplers at tower sites across NA as part of the NOAA GGGRN. These samples are collected at a higher sampling frequency (~daily) and are analyzed at NOAA by GC/MS[11]. Reported molar ratios for propane are based on a suite of gravimetric standards prepared at NOAA; calibration consistency is maintained independently from INSTAAR. The resulting NOAA calibration scale for propane has been assessed in an international round-robin exercise and was found to be consistent within 5% to other internationally-recognized and well established scales[12].

Data processing. At the time of the data processing final data from all considered sites until June 2014 (2014.5) were available, which was used as the cutoff of the analyses. The criterion

for individual sites data to be included was that data were available for at least 50% of the sampling days for 2009.5–2014.5. Two flask network and three tower site data sets were excluded because they did not meet this criterion. Similarly, *in-situ* data from remote monitoring sites were included if data were available for at least 50% of the 2009.5 – 2014.5 sampling dates.

NMHC data were first filtered for outliers; values that deviated more than 2 σ from a running median were excluded from trend analyses. Filtered data were then uploaded to the NOAA server for filtering and trend determination using the method of [13] and described at http://www.esrl.noaa.gov/gmd/ccgg/mbl/crvfit/crvfit.html. The first step is to fit a function, consisting of the sum of a polynomial and four harmonics (amplitude and phase of 1 through 4 cycles per year). The residuals of the function fit are smoothed by two low-pass filters, one for the trend (1.1 year full width at half-maximum, FWHM) and one for anomalies of the seasonal cycle (FWHM 50 days). The function and filtered data are then combined to generate a smoothed data curve, trend curve, a detrended seasonal cycle, seasonal amplitude, a polynomial fit, and the long-term growth rate. The smoothed data curve is a combination of the function and the short-term filter of the residuals. The trend curve is the polynomial part of the function plus the long-term filtered residuals, and represents the growth or decline of the data with the seasonal oscillations removed. The detrended seasonal cycle is complementary to the trend curve; it is the interannually varying cycle with the trend removed. The seasonal amplitude is the amplitude of the detrended seasonal cycle, and the growth rate is the rate of increase or decrease of the trend, found by taking the first derivative of the trend. Results of a trends statistical significance test are included in Tables S1 and S2. To avoid a bias from oversampling of the trend curve, its output was sampled only at times when retained flask data were available. These data were then subjected to the Mann-Kendall test[14] using a significance value of $\alpha = 0.01$. Results (calculated P-values) are presented in column 12 of Tables S1 and S2. Values < 0.01 reflect the rejection of the null-hypothesis that there is no trend. In these cases, the trend is found to be true at 99% confidence. Incidences where trends were found to be not statistically significant are listed in italics font and in brackets. Results show that for 33 NH ethane trend series (flask and in-situ), 31 show a positive trend. All positive trends are statisti-

cally significant. Lac La Biche, Alberta (LLB), shows a slight, non-significant negative trend. The LLB series has a reduced data coverage (73%), a high number of outlier points, and an $R^2 = 0$ result, all of which reduce the robustness of the LLB trend result. The other site showing a negative trend is Black Sea, Constanta (BSC). Similar to LLB, this site suffers from reduced data coverage (50%), and a high number of outlier points. This site appears to be severely impacted by nearby pollution sources. Despite these two sites showing rather noisy records and poor regression results, they were retained in the presentation of our results, as we did not want to use arbitrary filtering criteria.

The data used in the maps (Figure 3) were generated by applying a linear least squares fit of the trend data from each site for the period 2009.5–2014.5. The slope of the fit determined the color of the marker. The R^2 value times the coverage of the fit determined the size of the marker. The majority of the data are from NOAA/INSTAAR network flask sites. Furthermore, *in-situ* monitored sites were included, as well as propane data from tower sites.

EIC propane data were excluded because they showed influence from a local source. MWO propane data were excluded because a representative fit could not be drawn. A summary of trend results from all network flask, HATS, and *in-situ* observations is provided in Table S1 for ethane, and in Table S2 for propane.

Network flask – *in-situ* trend results evaluation. There is overlap of flask and *in-situ* VOC monitoring at two sites, i.e. SUM and HPB. The parallel observations at these two sites were used to evaluate the quality of the trend fit results from the weekly network flask measurements against the higher time resolution *in-situ* measurements. Details of these comparison studies will be presented in a forthcoming publication. In summary, these investigations showed that the less frequent flask records provide a good representation of the *in-situ* records, yielding trend results of the same magnitude (Figure 3).

Average ethane trend calculations. There are 47 sites that met the requirements (>50 % data coverage for 2009.5 – 2014.5) for inclusion in the trend analyses, with 31 of these sites in the NH. As can be seen in Tables S1, S2, data coverage, quality of the correlation analyses, and trend results vary widely. We explored a number of methods for deriving an average NH ethane

trend from these data. First, data from all sites, regardless of data coverage and quality of the regression fit, were treated equal. For sites with flask and *in-situ* data, the mean of both trend values was used (SUM and HPB). Sites were grouped by latitude zone, NH longitude, and continental/oceanic region, and average and median ethane trends were calculated from all sites within each region (Table S3). Please note the uneven representation of regions, as some of them have fewer sites than others, making results for regions with low representation less certain. Depending on the grouping and averaging, ethane trend results range from 3.5–4.3% yr^{-1} for the mean values and 2.9–4.2% yr^{-1} for the median results across all sub-regions. The lower mean values are largely due to the negative trend (-7.6% yr^{-1}) at BSC, a site that suffers from reduced data coverage (50%), and a high number of outliers, and appears to be severely impacted by nearby pollution sources (see above). Nonetheless, we kept the BSC result in the calculations for treating all sites equally for the NH mean trend calculations. Rates of increases are relatively high at Tiksi (TIK). Monitoring at TIK began in fall 2011, therefore the Tiksi record misses the first two years of the 2009.5 – 2014.5 window. The data coverage is just slightly above the 50% cutoff value (Tables S1 and S2). TIK is the site with the second lowest coverage of all sites that were included. Given the short record the uncertainty is much higher than for other sites.

Secondly, a mean NH ethane trend was calculated by weighing each individual trend result (Table M1) by the % coverage of the data, and the R^2 of the linear regression fit. For the two sites with flask and *in-situ* measurements the mean value of both trends, a 100% coverage value, and the sum of both R^2 values was used, to reflect the higher certainty from having two parallel results. The result of this analysis was a NH ethane increase rate of 4.7% yr^{-1}. This value is relatively strongly influenced by the two highest individual results from two sites in the central USA, i.e. Southern Great Plains, OK, with a rate of change of 10.7% yr^{-1} and Park Falls, WI, with a value of 7.9% yr^{-1}, also because both sites have full data coverage, and relatively high R^2 results. Removing these two sites reduces the mean NH ethane rate of change to 4.2% yr^{-1}. It is notable, though, that sites that are far distant from local influences, by horizontal separation, elevation, or by both, and located in the Atlantic Region, downwind of North America, showed the cleanest records, i.e. the highest correlation coefficient and on average relatively high rate of

change values. Sites that fall into these categories , (with their rate of change and R^2 results) are SUM (67.1 pmol, mol^{-1} yr^{-1}, 4.9% yr^{-1}, R^2 = 0.96 for flask results and 69.5 pmol mol^{-1} yr^{-1}, 5.6% yr^{-1}, R^2 = 0.67 for *in-situ*), ICE (46.2 pmol $mol^{-1}yr^{-1}$, 3.4% yr^{-1}, R^2 = 0.86), MHD (53.1 pmol mol^{-1} yr^{-1}, 4.3% yr^{-1}, R^2 = 0.65), AZR (86.7 pmol, mol^{-1} yr^{-1}, 7.7% yr^{-1}, R^2 = 0.57), ASK (72.9 pmol mol^{-1} yr^{-1}, 7.4% yr^{-1}, R^2 = 0.95), IZO (72.9 pmol mol^{-1} yr^{-1}, 7.4% yr^{-1}, R^2 = 0.95), and CVO (43.9 pmol mol^{-1} yr^{-1}, 5.4% yr^{-1}, R^2 = 0.85). The mean weighted ethane rate of change from these North Atlantic sites accounts to 5.5% yr^{-1}. These comparisons point towards highest rates of ethane increase in the central to eastern USA, followed by the North Atlantic region.

The overall hemispheric ethane trend result of 4.7% yr^{-1} from the latter method using R^2 * coverage as a weighing factor is 0.4 – 1.8% yr^{-1} higher than the regional results presented in Table S3. This possibly reflects a bias in the calculation as it places lower weight on sites with flat trends and corresponding low R^2 results.

The uncertainty (0.9%) of the best estimate of the ethane NH rate of change was determined as ½ of the range of the lowest (2.9%) to the highest value (4.7%) of the different types of regional trend determinations.

NMHC surfaces. Graphs in Figure 2 were derived using weekly data from the GGGRN sites. To reduce noise in the latitudinal distribution due to synoptic-scale atmospheric variability, records were fitted with a smooth curve[13]. We then used a data extension methodology[15] with important revisions[16] to produce a set of smoothed records, which are synchronized in time and have no temporal gaps. For each synchronized weekly time step, a latitude distribution (mole fraction versus sine of latitude) was constructed. Each value in the weekly distribution was assigned a relative weight using a strategy that assigns greater significance to sites with high signal-to-noise and consistent sampling. A curve was then fitted to each weekly weighted latitudinal distribution[17]. Finally, values were extracted from each weekly latitudinal fit at intervals of 0.05 sine of latitude from 90°S to 90°N and joined together to create the 2-dimensional matrix (time versus latitude) of molar ratios.

FTIR column observations. FTIR total and partial column data were derived from ongoing NDACC (www.ndacc.org) observations from solar viewing FTIR instruments. The network in-

struments are calibrated to common standards to ensure consistent optical performance across the network and over time. High-resolution mid-infrared solar radiation is recorded on a near daily basis. Analyses of the JFJ ethane retrieval and time series are presented in [18]. An improved retrieval approach delivers enhanced information content and sensitivity up to ~20 km altitude, providing two independent partial column time series, for the 3.58-8 and 8-21 km altitude. The ethane retrieval used for the Lauder spectra is presented in [19]. Initial analyses of Lauder time series are described in [20], where SH decreasing trends are given up to 2009. The statistical bootstrap resampling tool used for the trend calculations is presented in [21]. It determines a linear trend and corresponding uncertainties while accounting for the seasonal/intra-annual variability of the data. Determination of the uncertainty in the ethane column trend of the JFJ time series is explained in [18] . Several settings were tried (i.e. adjusting the step and integration interval) for the running mean calculations at JFJ and other NH FTIR sites (e.g. Toronto), always coming up with an ethane trend reversal date close to late 2008 - early 2009.

Emissions inventory. The ethane emissions inventory is a best estimate based on three different resources that build on other previous inventories and publications:

1. Based on reconstructed ambient air histories Aydin et al.[22] developed a year 2000 global ethane emission estimate of 8-10 Tg yr^{-1}. These authors do not differentiate between NH and SH emissions. Approximately 85% of ethane is estimated to be emitted in the NH (see 2. and 3. below). Based on that the global[22] estimate translates to 7-9 Tg yr^{-1} of NH ethane emissions.
2. We evaluated the inventory developed for the Hemispheric Transport of Air Pollutants, Phase II (HTAP2), which is a composite of regional inventories harmonized to represent 2008 and 2010[23]. Additional ethane emissions included in these simulations are biogenic emissions from the MEGAN2.1[24], and fire emissions from FINNv1.5[25]. Simulations with CAM-chem indicated that the anthropogenic emissions needed to be doubled to match the pre-2009 NMHC FTIR observations at JFJ. A summary of these adjusted emissions by region and sources is given in Table S4 for 2007. Year 2009.5 NH ethane emissions are estimated as 15 Tg yr^{-1} from the 'Globe –all' minus the SH emissions.

3. The RCP85 database (Representative Concentration Pathway 8.5[26,27] includes total emissions of ethane of ~12.9 Tg yr^{-1}, of which 0.53, 2.3 and 10 Tg yr^{-1} are emitted from biogenic, biomass burning and anthropogenic sources, respectively. 9.9 Tg yr^{-1} of the total 12.9 Tg yr^{-1} are emitted in the NH.

We used 9.9 Tg yr^{-1}, which is the middle value of these three estimates for the ethane, NMHC, and methane emission increase, and ozone sensitivity modeling, and 1/2 of the minimum (7 Tg yr^{-1}) to maximum (15 Tg yr^{-1}) range as uncertainty interval (4 Tg yr^{-1}).

Scaling of methane to ethane. The methane/ethane emission ratio was determined as the median of available data from analyses of both compounds in USA O&NG regions (Table S5). We use 1/2 of the difference between the minimum and maximum value in the data as uncertainty interval (5.6). The methane emission estimation uncertainty interval was calculated by error propagation including uncertainties in the ethane growth rate, the ethane inventory emission, and the methane/ethane ratio.

Scaling of total NMHC to ethane calculation. There are few publications that report speciated NMHCs, and there are even fewer that include ethane, from O&NG source regions. Furthermore, some of the available literature studies suffer from measurements being influenced to variable degree by other contributing sources. We compiled published speciated NMHC/ethane emission ratios from O&NG development areas in Table S6. Ambient air measurements were converted to relative mass emission ratios scaled to ethane. The contribution of missing NMHC to the total NMHC emission > C_2 was estimated by adding up the relative fractions of missing species reported in the [28] study and pro-rating the contribution of the missing species. There is a considerable amount of variability in these data, likely determined by the different NMHC emission ratios in different shale regions.

Among these data sets results from the Uintah Basin are likely of a relatively high representativeness for several reasons: 1. Despite the Uintah Basin having a low population density atmospheric VOC have been found to be highly elevated, dominated by emission from O&NG operations. In 2013 the basin had an estimated 4300 oil and 6900 gas producing wells, therefore emissions reflect a combination of both types of wells. 2. This dataset is the average over two

campaigns from two subsequent years. 3. Measurements represent an overall high number of samples. 4. Data are from surface and tethered balloon measurements from January – February, when relatively shallow boundary layer conditions prevailed, which fostered accumulation of nearby emissions.

The mean and median values for $\Sigma E_{NMHC>C2}/E_{ethane}$ from these studies were calculated as 2.47 and 1.85, respectively, with the Uintah Basin result being the medium value. For the reasons detailed above, we chose a Uintah median value as $\Sigma E_{NMHC>C2}/E_{ethane}$ scaling factor. The uncertainty of 1.4 was determined as 0.5 times the range of minimum to maximum scaling factors from individual studies. Uncertainty of the scaled total NMHC emission was calculated by error propagation.

Ozone Modeling. EMAC (ECHAM5/MESSy for atmospheric chemistry version 2.50[29]) was used to develop of first order of magnitude estimation of the impact of the emissions increase of simple NMHC on ozone formation. While most likely the majority of the added ethane flux is from the USA, other global regions may potentially have contributed to the flux increase. To reflect this uncertainty we applied lower estimates for several of the applied variables: 1. We did not consider an increase in methane emissions on ozone production. 2. We only considered estimated associated emissions of C2-C5, excluding NMHC > C5, which constitute ~10% of the total O&NG NMHC emission (Table M6), and on average have higher reactivity and ozone production potential than the lighter NMHC. Furthermore, the scaling value applied here is below the mean of available observations (Table S6). 3. The applied ethane NH inventory flux of 9.9 Tg yr^{-1} is a significantly lower value compared to the most recent estimate (15 Tg yr^{-1}, as explained above and in [30]). The model set-up was the same as in [27], with the only exception of an augmented chemical scheme, which includes decomposition chemistry of simple hydrocarbons (i.e. *n/i*-butane and *n/i*-pentane)[31]. The model simulations adopted emissions from the RCP85 database (Representative Concentration Pathway 8.5)[26,27]. Two simulations were performed for 2009.5-2014.5: 1. with constant NMHC emissions, named CONST, and 2. with increasing NMHC, named TREND. To disentangle the impact of increased NMHC emissions, all other tracer emissions were kept constant. We applied a trend of 4.2% yr^{-1} for the NH emissions of ethane over

five years based on the JFJ FTIR mid-troposphere column trend value. In the model NH emissions of ethane are ~9.9 Tg yr^{-1}, of which 0.17, 0.9 and 8.8 Tg yr^{-1} are emitted from biogenic, biomass burning and anthropogenic sources, respectively. Therefore, the ethane growth rate accounts to an increase in ethane emission O&NG sources of ~0.41 Tg yr^{-1}. Based on observed ambient air relative ratios of NMHC in source regions, see Table S6, 0.30, 0.11, 0.08, 0.05 and 0.06 Tg yr^{-1} increases were prescribed to propane, *n*-butane, *i*-butane, *n*-pentane and *i*-pentane, every year for five years, so that after five years the total emission increase was five times these listed emissions. Uncertainties in all scaling ratios propagate into the calculated ozone changes. The emissions map was based on shale O&NG wells distribution, available at http://frack.skytruth/org. Information used for generating this map is based on "voluntary disclosure reports submitted by oil and gas drilling operators" and relies on locations of more than 15,000 wells. We assumed that all wells emit the same amounts of NMHC, neglecting difference in wells size. Finally, the distributed map of the wells was aggregated in a 0.5 x 0.5 degree regular map, and emissions were scaled based on the well number density in each grid cell. The resulting emissions map, see Figure S1, identifies regions that have experienced recent growth of O&NG development, with regions of large emission increases in the central and northeastern USA.

Modeling results in Figure 4 show the differences in the ozone molar fraction between model results from the simulation CONST and TREND. Please note that these results are based on constant emissions of other precursors, including those of nitrogen oxides (NO_x). Decreasing trends of NO_x over the USA and of VOC in urban areas have led to a general decrease of ozone in many urban regions. Omission of these effects will cause a high bias of the ozone changes that were calculated here. Consequently, these model results should be considered as preliminary results, providing an indication of the direction of ozone effects from added O&NG emissions and taken as motivation for more in depth modeling of the net effect resulting from these emission changes.

References cited in Methods

1 Pollmann, J., Helmig, D., Hueber, J., Plass-Dülmer, C. & Tans, P. Sampling, storage, and analysis of C2-C7 non-methane hydrocarbons from the US National Oceanic and Atmospheric Administration Cooperative Air Sampling Network glass flasks. *J. Chrom. A* **1188**, 75-87 (2008).
2 Helmig, D. *et al.* Volatile Organic Compounds in the Global Atmosphere. *Eos Trans. AGU* **90** (2009).
3 WCC-VOC. Karlsruhe Institute of Technology. *http://www.imk-ifu.kit.edu/wcc-voc/* **2015**, Accessed February 2016 (2016).
4 WMO. A WMO/GAW Expert Workshop on Global Long-Term Measurements of Volatile Organic Compounds (VOCs). *WMO Report No. 171* Geneva, Switzerland, 30 January to 1 February 2006, 36 pp. (2007).
5 Pollmann, J., Helmig, D., Hueber, J., Tanner, D. & Tans, P. P. Evaluation of solid adsorbent materials for cryogen-free trapping - gas chromatographic analysis of atmospheric C2-C6 non-methane hydrocarbons. *J. Chrom. A* **1134**, 1-15 (2006).
6 Global-VOC. http://instaar.colorado.edu/arl/Global_VOC.html. **Accessed Oct. 2015** (2014).
7 Helmig, D., Stephens, C. R., Caramore, J. & Hueber, J. Seasonal behavior of non-methane hydrocarbons in the firn air at Summit, Greenland. *Atmos. Environ.* **85**, 234-246, doi:http://dx.doi.org/10.1016/j.atmosenv.2013.11.021 (2014).
8 Plass-Duelmer, C., Michl, K., Ruf, R. & Berresheim, H. C-2-C-8 hydrocarbon measurement and quality control procedures at the Global Atmosphere Watch Observatory Hohenpeissenberg. *J. Chrom. A* **953**, 175-197, doi:10.1016/s0021-9673(02)00128-0 (2002).
9 Miller, B. R. *et al.* Medusa: A sample preconcentration and GC/MS detector system for in situ measurements of atmospheric trace halocarbons, hydrocarbons, and sulfur compounds. *Anal. Chem.* **80**, 1536-1545, doi:10.1021/ac702084k (2008).
10 Read, K. A. *et al.* Intra-annual cycles of NMVOC in the tropical marine boundary layer and their use for interpreting seasonal variability in CO. *J. Geophys. Res.* **114**, doi:10.1029/2009jd011879 (2009).
11 Pétron, G. *et al.* Hydrocarbon emissions characterization in the Colorado Front Range: A pilot study. *J. Geophys. Res.* **117**, 1-19, doi:10.1029/2011jd016360 (2012).
12 Rhoderick, G. C. *et al.* International comparison of a hydrocarbon gas standard at the picomol per mol level. *Anal. Chem.* **86**, 2580-2589, doi:10.1021/ac403761u (2014).
13 Thoning, K. W., Tans, P. P. & Komhyr, W. D. Atmospheric carbon-dioxide at Mauna Loa observatory .2. analysis of the NOAA GMCC data, 1974-1985. *J. Geophys. Res.* **94**, 8549-8565, doi:10.1029/JD094iD06p08549 (1989).
14 Yue, S., Pilon, P. & Cavadias, G. Power of the Mann-Kendall and Spearman's rho tests for detecting monotonic trends in hydrological series. *J. Hydrol.* **259**, 254-271, doi:10.1016/s0022-1694(01)00594-7 (2002).
15 Masarie, K. A. & Tans, P. P. Extension and integration of atmospheric carbon-dioxide data into a globally consistent measurement record. *J. Geophys. Res.* **100**, 11593-11610, doi:10.1029/95jd00859 (1995).
16 GLOBALVIEW-CO2. Cooperative Atmospheric Data Integration Project - Carbon Dioxide. CD-ROM, NOAA ESRL, Boulder, Colorado *ftp.cmdl.noaa.gov, Path: ccg/co2/GLOBALVIEW* (2011).
17 Tans, P. P., Conway, T. J. & Nakazawa, T. Latitudinal distribution of the sources and sinks of atmospheric carbon-dioxide derived from surface observations and an atmospheric transport model. *J. Geophys. Res.* **94**, 5151-5172, doi:10.1029/JD094iD04p05151 (1989).
18 Franco, B. *et al.* Retrieval of ethane from ground-based FTIR solar spectra using improved spectroscopy: Recent burden increase above Jungfraujoch. *Journal of Quantitative Spectroscopy & Radiative Transfer* **160**, 36-49, doi:10.1016/j.jqsrt.2015.03.017 (2015).

19 Rinsland, C. P. *et al.* Multiyear infrared solar spectroscopic measurements of HCN, CO, C2H6, and C2H2 tropospheric columns above Lauder, New Zealand (45°S latitude). *Journal of Geophysical Research: Atmospheres* **107**, ACH 1-1-ACH 1-12, doi:10.1029/2001JD001150 (2002).
20 Zeng, G. *et al.* Trends and variations in CO, C2H6, and HCN in the Southern Hemisphere point to the declining anthropogenic emissions of CO and C2H6. *Atmos. Chem. Phys.* **12**, 7543-7555, doi:10.5194/acp-12-7543-2012 (2012).
21 Gardiner, T. *et al.* Trend analysis of greenhouse gases over Europe measured by a network of ground-based remote FTIR instruments. *Atmos. Chem. Phys.* **8**, 6719-6727 (2008).
22 Aydin, M. *et al.* Recent decreases in fossil-fuel emissions of ethane and methane derived from firn air. *Nature* **476**, 198-201, doi:10.1038/nature10352 (2011).
23 Janssens-Maenhout, G. *et al.* HTAP_v2: a mosaic of regional and global emission gridmaps for 2008 and 2010 to study hemispheric transport of air pollution. *Atmos. Chem. Phys.* **15**, 12867-12909 (2015).
24 Guenther, A. B. *et al.* The Model of Emissions of Gases and Aerosols from Nature version 2.1 (MEGAN2.1): an extended and updated framework for modeling biogenic emissions. *Geoscientific Model Development* **5**, 1471-1492, doi:10.5194/gmd-5-1471-2012 (2012).
25 Wiedinmyer, C. *et al.* The Fire INventory from NCAR (FINN): a high resolution global model to estimate the emissions from open burning. *Geoscientific Model Development* **4**, 625-641, doi:10.5194/gmd-4-625-2011 (2011).
26 Riahi, K., Grübler, A. & Nakicenovic, N. Scenarios of long-term socio-economic and environmental development under climate stabilization. *Technological Forecasting and Social Change* **74**, 887-935, doi:http://dx.doi.org/10.1016/j.techfore.2006.05.026 (2007).
27 Pozzer, A. *et al.* AOD trends during 2001–2010 from observations and model simulations. *Atmos. Chem. Phys.* **15**, 5521-5535, doi:10.5194/acp-15-5521-2015 (2015).
28 Swarthout, R. F., Russo, R. S., Zhou, Y., Hart, A. H. & Sive, B. C. Volatile organic compound distributions during the NACHTT campaign at the Boulder Atmospheric Observatory: Influence of urban and natural gas sources. *J. Geophys. Res.* **118**, 10614-10637 (2013).
29 Jöckel, P. *et al.* Development cycle 2 of the Modular Earth Submodel System (MESSy2). *Geosci. Model Dev.* **3**, 717-752, doi:10.5194/gmd-3-717-2010 (2010).
30 Franco, B. *et al.* Evaluating ethane and methane emissions associated with the development of oil and natural gas extraction in North America. *Environ. Res. Lett. 11,* 0440010 (2016).
31 Pozzer, A. *et al.* Observed and simulated global distribution and budget of atmospheric C2-C5 alkanes. *Atmos. Chem. Phys.* **10**, 4403-4422, doi:10.5194/acp-10-4403-2010 (2010).

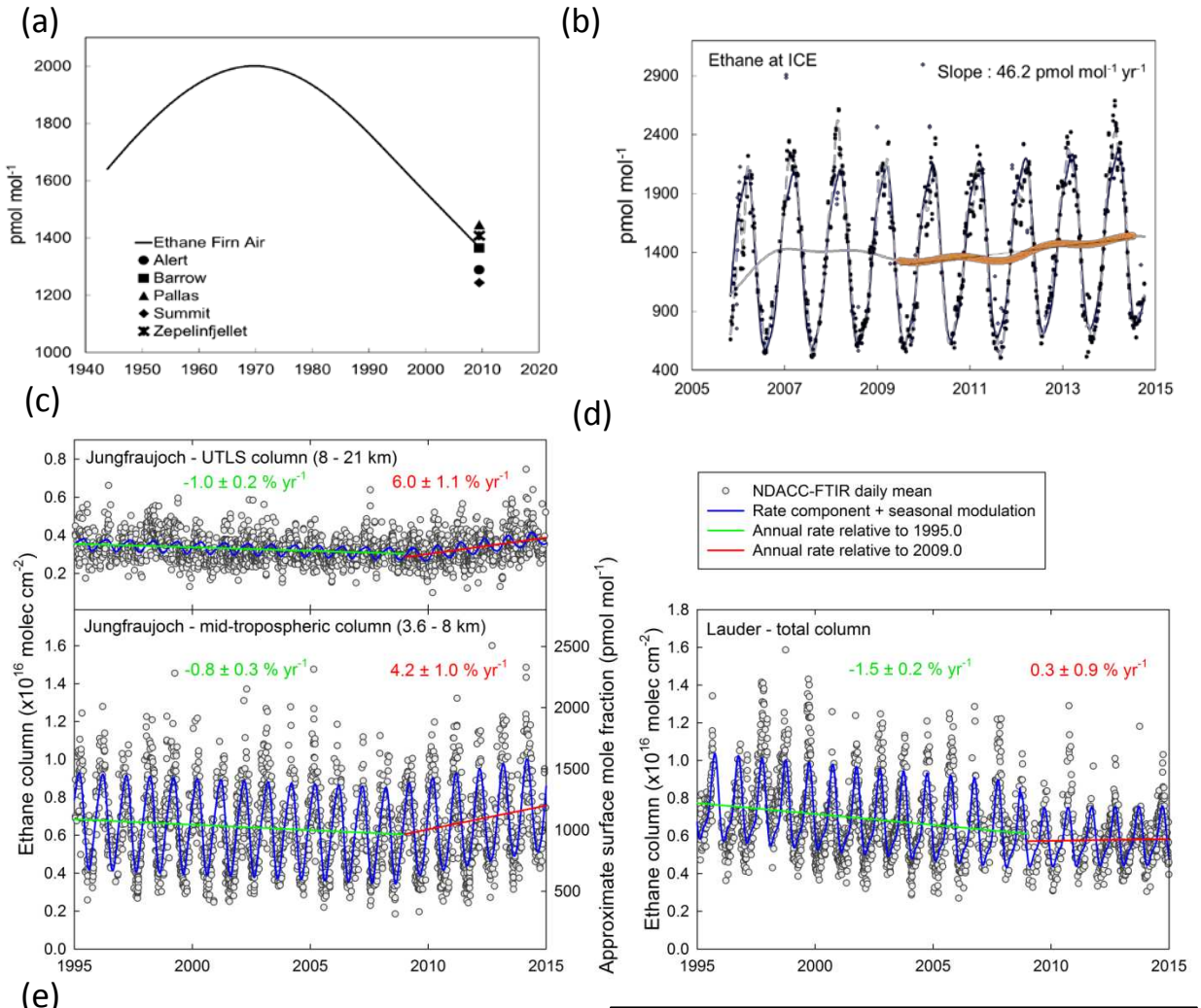

Figure 1. Histories of atmospheric ethane. (a) Reconstructed 1950-2010 ethane history from firn air sampling at NEEM in Greenland with 2009.5 mean seasonally detrended atmospheric values at five arctic sites for comparison[1]. (b) Ten years of NMHC flask network data in South Iceland. Shown are individual flask data, identified outliers (small points), a smoothed fit and the trend results after removal of harmonic components, and the linear regression fit, with a 46.2 pmol mol^{-1} yr^{-1} increase from 2009.5 to 2014.5. (c, d) Ethane FTIR columns showing a trend reversal and increasing rate of change after 2009 at Jungfraujoch, Switzerland, in contrast to Lauder, New Zealand. (e) Monthly running median data from the daily in-situ record at Hohenpeissenberg, with smoothed, function, and trend fits. A polynomial fit shows a minimum in the second half of 2009; the linear regression to the post 2009.5 trend curves and seasonal maxima and minima show increases of 22-23 pmol mol^{-1} yr^{-1}.

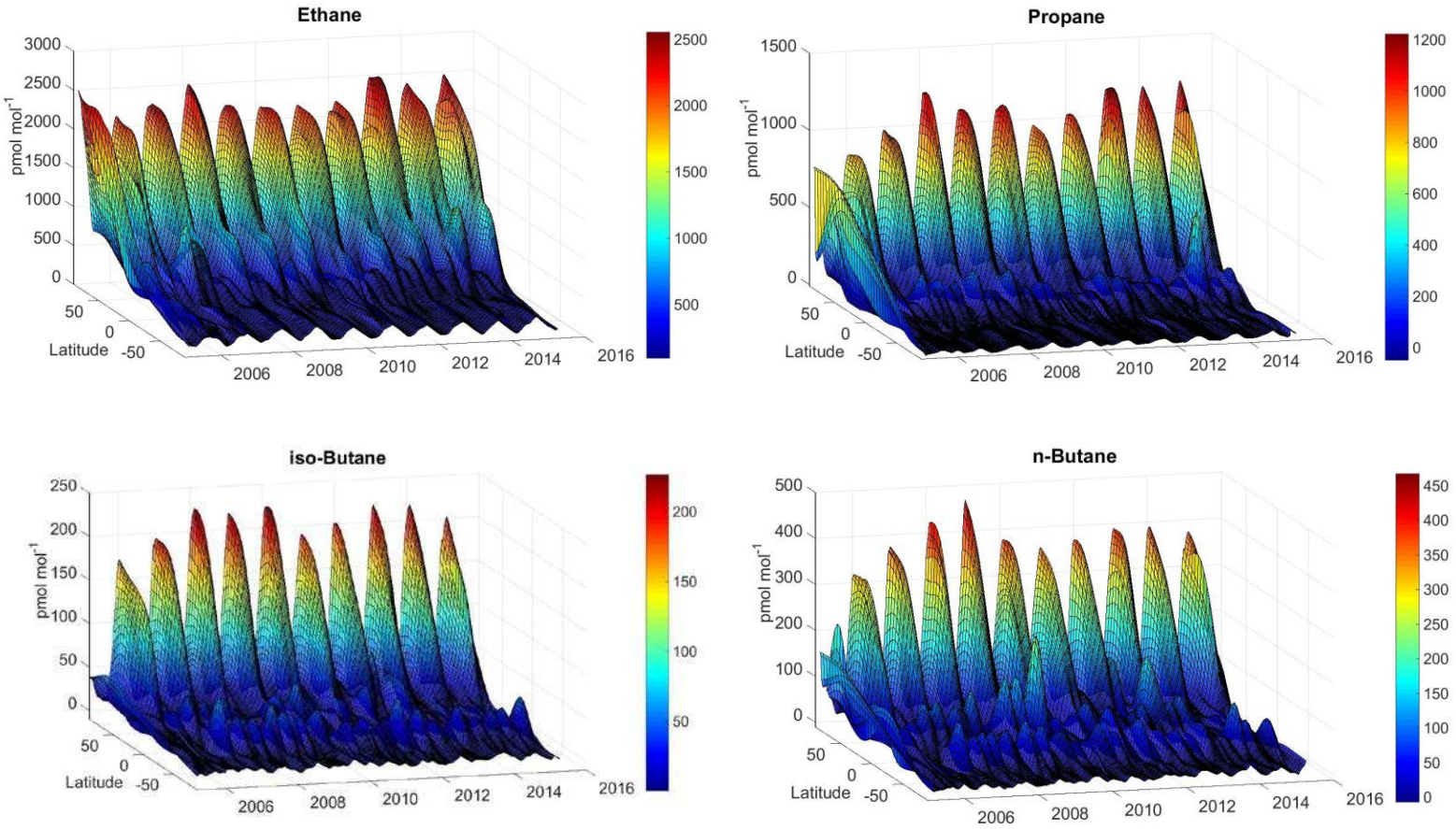

Figure 2 | **Latitudinal distribution of ethane, propane, *iso*-butane, *n*-butane**. These representations of surface mixing ratios were generated using weekly data from 37-39 global background monitoring sites, altogether some 30,000 data points for each graph. Please note that these plots are a representation of latitudinal averages of atmospheric mixing ratios; therefore, they do not capture differences between continents at the same latitude. Procedures for data filtering and processing are discussed in the Methods Section.

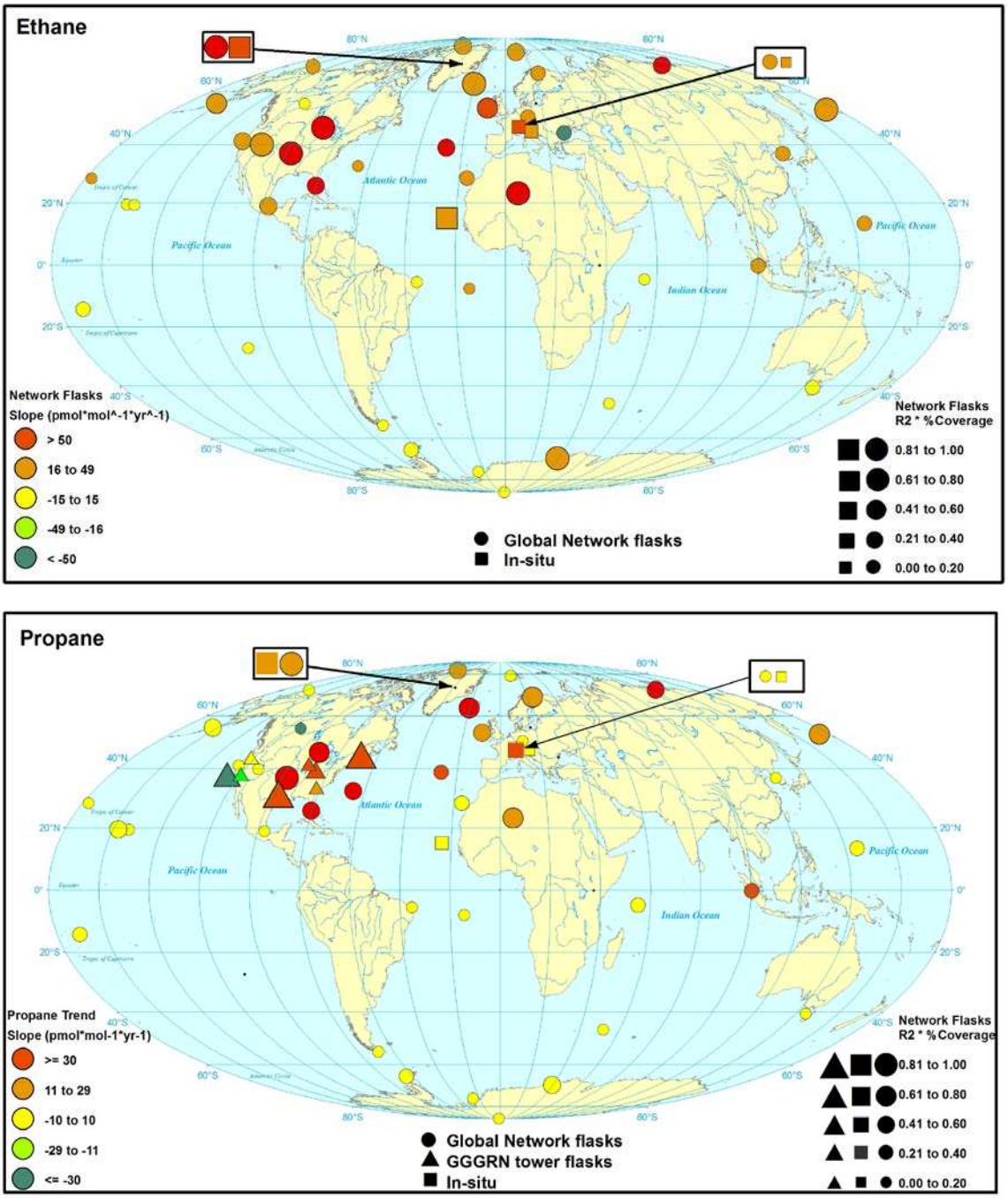

Figure 3 | **Ethane and propane trends at global monitoring sites.** Ethane increases are given by the color scale with marker size corresponding to the R^2 of the fit multiplied by the fraction of available site data. Overlapping flask and *in-situ* results are shown in black boxes for Summit and Hohenpeissenberg. (a) For ethane, increasing ethane is observed throughout the NH, with the strongest signal in North America, the North Atlantic, and neighboring continents. There is no, or only little change in ethane at SH sites. (b) Propane shows a more pronounced region of increasing mole fractions in the eastern USA and at nearby downwind sites. Again, these changes are not seen at the SH sites.